



Biosiliceous and geochemical response to biotic and climatic events in the Palaeocene

Cécile Figus^{1,2}, Steve Bohaty³, Johan Renaudie⁴, and Jakub Witkowski¹

¹Institute of Marine and Environmental Sciences, University of Szczecin, 70-383 Szczecin, Poland

²Doctoral School, University of Szczecin, 70-383 Szczecin, Poland

³Institute of Earth Sciences, University of Heidelberg, 69120, Heidelberg, Germany

⁴FBI Dynamik der Natur, Museum für Naturkunde, 10115 Berlin, Germany

Correspondence: Cécile Figus (cecile.figus@phd.usz.edu.pl)

Abstract. Hyperthermal events are a key element in understanding Palaeogene climate history, but many of these events outside of prominent Palaeocene Eocene Thermal Maximum are poorly understood and studied. Two hyperthermal events that occurred in the middle to late Palaeocene include the Latest Danian Event (LDE) and the Early Late Palaeocene Event (ELPE). Most studies of these events focus on calcareous nannofossils and foraminifera, as well as geochemical data and astronomical tuning, but, to date, none consider biosiliceous production and flux. We therefore present eight records of biosiliceous fluxes, supported by geochemical data, from the Atlantic, Pacific and Indian ocean sites spanning the Palaeocene. Our results show pronounced variability in biosiliceous fluxes through the Palaeocene, with a peak at the time of the LDE. Establishing a link between the ELPE and biosiliceous flux variability through this time interval is more challenging, but the occurrence of peaks in biosiliceous fluxes after this event may indicate a global response of biogenic silica to the ELPE.

1 Introduction

The study of Palaeogene climates (~66 to ~23 Ma) includes a focus on intense short-term (up to ~400,000 years; Barnet et al., 2019) climatic events called ‘hyperthermals’, which are often compared to the present-day climate change in terms of greenhouse gas emissions into the atmosphere (Foster et al., 2018; Kiessling et al., 2024). These hyperthermal events are associated with, among other characteristics, rapid (between 1,000 and 100,000 year duration) increases in temperature and atmospheric CO₂, as well as ocean acidification (Bowen et al., 2004; Foster et al., 2017; Westerhold et al., 2018). The most widely known hyperthermal event is the Palaeocene-Eocene Thermal Maximum (PETM; ~56 Ma) (Kennett and Stott, 1991; McInerney and Wing, 2011), when large volumes of isotopically depleted carbon were released into the oceans and atmosphere over the course of ~10,000 years (Penman et al., 2014). Although the PETM is a hallmark of the Palaeogene greenhouse climates, it is not the only short-lived climate event that took place during the Palaeogene. The early Cenozoic was characterized by an initial extreme warmth following the K/Pg massive extinction, before a global cooling of the climate from ~53 Ma onwards. Several climatic events occurred during the early Palaeogene (Littler et al., 2014; Barnet et al., 2019; Westerhold et al., 2020) such as the Early Eocene Climate Optimum (EECO; ~53 to ~49 Ma) (Zachos et al., 2008).



Two short-lived climatic events, which are particularly understudied, occurred in the Palaeocene (~66 to ~56 Ma): the Latest Danian Event (LDE; ~62.2 Ma) and the Early Late Palaeocene Event (ELPE, also known as the Mid-Palaeocene Biotic Event or MPBE; Bernaola et al., 2007). Published ages for the ELPE range from ~58.4 Ma (Bralower et al., 2002; Petrizzo, 2006) to ~59.5 Ma (Li et al., 2024). In addition, the qualification of the ELPE as a hyperthermal event has long been debated (Littler et al., 2014), as it is characterized by several changes in the biota and environment (Coccioni et al., 2019), but evidence for a negative carbon isotope excursion (CIE) or warming is not present in all $\delta^{18}\text{O}$ and $\delta^{13}\text{C}$ records spanning this interval (Hollis et al., 2022; Li et al., 2024). The LDE, in contrast, is associated with the largest negative CIE in the Palaeocene (Bornemann et al., 2009; Dinarès-Turell et al., 2012), and has been linked to enhanced volcanic activity (Jehle et al., 2015).

Reconstructing long- and short-term palaeoclimatic changes is possible using numerous proxies (e.g., Froelich and Misra, 2014; Jehle et al., 2015; Westerhold et al., 2018, 2020), such as $\delta^{18}\text{O}$ (for ice volume and temperature) or $\delta^{13}\text{C}$ (for the carbon cycle), but also through the use of biogenic opal records. Fossil diatoms and radiolarians are remnants of skeletons in opal, amorphous or crystallized depending on the stage of diagenetic transformation (Rice et al., 1995; Yanchilina et al., 2020), and thus are part of the biosiliceous fraction contained in marine sediments. Based on a compilation of data from deep-sea diatom-bearing sites in the Atlantic, Pacific and Indian oceans, Figus et al. indicate no apparent biosiliceous flux response to Palaeocene hyperthermal events, while the stratigraphic distribution of shallow marine diatomite deposited in epicontinental seas during this period does suggest a link between certain hyperthermal events (e.g., the PETM) and diatomite accumulation (Figus et al., 2024). However, compiling stratigraphic data from deep-sea sites drilled by the Deep Sea Drilling Project (DSDP) campaigns and its successors has revealed an uneven distribution of the number of sites containing Palaeogene biosiliceous sediments, with a lower number of sites covering the Palaeocene, as well as a bias in the preservation of early Cenozoic siliceous microfossils (Figus et al.). We therefore decided to focus on Palaeocene signals (between ~63 and ~62 and between ~60 and ~57 Ma) in opal fluxes and geochemical data at eight deep-sea sites drilled in the Atlantic, Pacific and Indian Ocean. The new records produced for this study are compared with published data to reconstruct the trends in biosiliceous fluxes across these two intervals, and to investigate a possible link with the LDE and ELPE.

2 Materials and methods

2.1 Site selection

The eight sites selected for this study are located in the North and South Atlantic, South Pacific and Indian Ocean (Table 1, Fig. 1). We focused on sites that contain abundant and/or well-preserved diatoms as documented in DSDP and Ocean Drilling Program (ODP) reports, including DSDP sites 208 and 384 and ODP sites 1050, 1051 and 1121. The Palaeocene sequences recovered at these sites also contain abundant radiolarians over the entire section analyzed in this study.

Site selection was also determined by the stratigraphic span of the sediments, i.e., we specifically targeted intervals expected to include a record of the LDE and ELPE. The age-depth models used for each site were updated to GTS2012 (Gradstein et al., 2012), based on Renaudie et al. (2018) for 700B, 752A and 1121B, and Witkowski et al. (2020) for the remaining sites.



Table 1. Sites included in this study, with geographical coordinates, location and drilling report reference.

Site/Hole	Coordinates	Location	Reference
208	26°06.61'S, 161°13.27'E	South Pacific	Shipboard Scientific Party (1973)
384	40°21.65'N, 51°39.80'W	North Atlantic	Shipboard Scientific Party (1979)
700B	51°31.977'S, 30°16.688'W	South Atlantic	Shipboard Scientific Party (1988)
752A	30°53.475'S, 93°34.652'E	Indian Ocean	Shipboard Scientific Party (1989)
1050A	30°05.9977'N, 76°14.1011'W	North Atlantic	Shipboard Scientific Party (1998a)
1050C	30°05.9953'N, 76°14.0997'W	North Atlantic	Shipboard Scientific Party (1998a)
1051A	30°03.1740'N, 76°21.4580'W	North Atlantic	Shipboard Scientific Party (1998b)
1121B	50°53.8740'S, 176°59.8620'E	South Pacific	Shipboard Scientific Party (2000)

55 2.2 Stable isotope analysis

Stable isotope analysis of bulk carbonates was carried out on samples from sites 700B, 752A and 1121B. Each sample of bulk sediment was freeze-dried and then ground using a mortar and pestle. 50 to 100 μg of pulverized sediment was analyzed for carbon and oxygen isotope stable isotope ratios using a Thermo Scientific Kiel IV Carbonate device coupled with a MAT253 isotope ratio mass spectrometer at Heidelberg University (Laboratory for Stable Isotope Mass Spectrometry). The $\delta^{13}\text{C}$ and $\delta^{18}\text{O}$ results (expressed in per mil, ‰) were normalized and calibrated against the Vienna Pee Dee Belemnite (VPDB) standard (see Fig. 2 and full results in Supplementary Material Table S4).

2.3 Biogenic opal determination

The samples underwent silica extraction following the Olivarez Lyle and Lyle (2002) protocol, modified for this study (we used 1M KOH and 10 mg sediment subsamples, instead of 2M KOH and 20 mg subsamples indicated in the original protocol). This modification aims to avoid silica polymerization, as described in Witkowski et al. (2021). The concentrations of biogenic opal in each sample were then determined by heteropoly blue method (Hach method 8186) on a Hach DR-3900 spectrophotometer.

The results obtained were used to calculate the percentage weight of opal per gram of sediment in each sample (see Supplementary Material Fig. S1) and the mass accumulation rate (Fig. 3), using the methods described in Witkowski et al. (2021).

2.4 Statistical treatment

The bioSiO_2 flux data produced for this study were linearly interpolated and smoothed using a cubic smoothing spline (Green and Silverman, 1994) in order to compare records between sites. A Pearson correlation coefficient and cross-correlation function were calculated on the smoothed bioSiO_2 flux data for each pair of sites. The supplementary Figs S2–22 show the regions of overlap between the site results and the smoothing spline after interpolation. In order to compare only the periods of interest for this study and to improve the significance of the results, cross-correlations were also applied focusing on the data



75 between 60 and 57 Ma (Supplementary Material Table S1), and between 63 and 62 Ma (Supplementary Material Table S2).
The results indicate the correlation between peak bioSiO_2 fluxes at different sites during these periods. Pearson coefficient and
cross-correlation function were also calculated between bioSiO_2 flux and percentage of CaCO_3 at each site (Supplementary
Material Table S3), to determine whether bioSiO_2 peaks between 60 and 57 Ma were correlated with carbonate dissolution
(see figures in the Supplementary Material Figs S23–28). The comparison between time series was carried out using R (R Core
80 Team, 2024).

3 Results and interpretation

Although both events are understudied, they are well defined in deep-sea sediments (Littler et al., 2014; Jehle et al., 2015).
Most studies of these events focus on calcareous nannofossils and foraminifers (e.g., Petrizzo, 2006; Sprong et al., 2012; Jehle
et al., 2015; Alegret et al., 2016), or on geochemical data and astronomical tuning (e.g., Westerhold et al., 2008; Littler et al.,
85 2014; Hilgen et al., 2015; Li et al., 2024), but, to date, siliceous microfossils and biosiliceous fluxes have not been investigated
with regard to these two events.

3.1 Biosiliceous and geochemical response to the LDE

In this study, the LDE is recorded around 62.2 Ma at Sites 208 (South Pacific), 700B (South Atlantic), 384, 1050C and 1051A
(North Atlantic). As $\delta^{13}\text{C}$ and $\delta^{18}\text{O}$ were measured only in Holes 700B, 752A and 1121B, and that the record at Hole 1121B
90 does not cover the LDE, we decided to use the isotopic data from Hollis et al. (2014) for Hole 1121B (South Pacific). The results
from Holes 700B and 1121B for the LDE interval are consistent with the negative CIE (Fig. 2b) and a short warming episode
(Fig. 2a) described in previous studies (Jehle et al., 2015, 2019; Alegret et al., 2016). Furthermore, Haq et al. (1979) explain
that while calcareous nannofossil assemblages indicate a cooling trend between ~61 and ~58 Ma at Site 384, assemblages
found around ~62 Ma suggest warming, which likely corresponds to the LDE.

95 All the bioSiO_2 flux records (Fig. 3) show a peak around the LDE, except for site 208 (Fig. 3d) which has a peak before
the LDE, followed by a drop at the time of the event. One possible explanation could be a problem in the calibration of
the data on GTS2012, causing a mismatch in the position of the peak. This hypothesis is supported by the cross-correlation
results, which show that the peak bioSiO_2 fluxes at each site throughout the LDE are correlated positively or negatively (i.e.,
Hole 700B is correlated negatively to other sites, while all the other sites are correlated positively with each other, except the
100 correlations between Holes 752A and 1121B, and Holes 1050A with 1051A). The intense carbon release and enhancement
of the hydrological cycle associated with these climatic events should be expected to enhance the chemical alteration and
mechanical erosion of rocks on land, and thus to manifest as elevated rates of silicate weathering (Berner et al., 1983; Penman
et al., 2019). The resulting input of dissolved silica—used by siliceous biota to build their exoskeletons—into the oceans
is increased (Penman, 2016), leading to a rise in the number of siliceous microfossils in sediments. However, one question
105 remains: why are these peaks not detected in the global compilation of deep-sea diatom-bearing sediments of Figus et al.?
The most plausible answers would be 1) the resolution of the dataset in Figus et al. and 2) the composition of the biosiliceous



content analyzed in the present study. In Figus et al., the data are computed with a temporal resolution of one million years, whereas the results of the current study are more precise. In addition, Figus et al. only consider the number of sites containing diatom-bearing sediments. The bioSiO_2 fluxes measured in this study are indifferent to the siliceous content of the sediments, whether they contain diatoms, radiolarians, or any other siliceous microfossil. It is therefore likely that radiolarians, more than diatoms, responded to the LDE.

3.2 Characterization of the ELPE

3.2.1 A climatic and/or biotic event?

The ELPE was described early on in the scientific drilling literature without being named, for example in DSDP reports such as for Site 384 (Shipboard Scientific Party, 1979), and has since been better identified with precise characteristics. Now recognized as a hyperthermal event, the ELPE was originally described as a carbonate dissolution event. To improve the identification of the ELPE, Petrizzo (2006) indicated a sequence of stages based on the study of planktonic foraminiferal assemblages at Shatsky Rise (northwest Pacific). These stages include the first occurrence and increase in abundance of the nannofossil *Heliolithus kleinpellii*, variations in the abundance of the planktonic foraminifera *Igorina tadjikistanensis* and *Igorina albeari*, a peak in magnetic susceptibility, and the deposition of phillipsite, a member of the zeolite group. In addition, the event seems to be associated with carbonate dissolution, probably related to a shoaling of the carbonate compensation depth (CCD) and the lysocline (Bralower et al., 2002; Petrizzo, 2006). Littler et al. (2014) explain this shoaling by a massive input of isotopically depleted carbon into the oceans during the ELPE. Bernaola et al. (2007) make the same observation, based on the occurrence of a negative CIE and a decrease in the $\delta^{18}\text{O}$ record at Zumaia, an onshore section in the Pyrenean basin. Several other studies report a negative ELPE-related CIE in shallow marine or terrestrial environments such as the eastern Tethys (Sarkar et al., 2022) and western Neo-Tethys (Coccioni et al., 2019), or two CIEs, as recorded in the Tethys Himalaya (Li et al., 2024) and northwest Argentina (Hyland et al., 2015). In the deep-sea, CIEs are reported from ODP Legs 198 (Shatsky Rise) and 208 (Walvis Ridge, South Atlantic) (Littler et al., 2014; Hilgen et al., 2015). Whereas these papers are in general agreement with the interpretation of the ELPE as a hyperthermal event, Hollis et al. (2014) provide a different explanation, correlating the ELPE with the onset of the Palaeocene Carbon Isotope Maximum (PCIM), and a climate cooling. According to Hollis et al. (2014), the decrease in carbonate content at ODP Site 1121B could be the result of regional cooling, linked to glacio-eustatic factors in the Antarctic region, enhancing upwelling and marine productivity during the ELPE.

3.2.2 Dating the ELPE

Although the ELPE is well constrained in the deep-sea, onshore sites appear to disagree with the timing of the event. At deep-sea sites, biostratigraphic and geochemical data first suggested that the ELPE occurred at ~58.4 Ma (Bralower et al., 2002; Petrizzo, 2006) or ~58.9 Ma (Littler et al., 2014). Revisions of these data by cyclostratigraphy, using magnetic susceptibility and iron content, place this event earlier, at the Selandian–Thanetian boundary, at ~59.2 Ma (Westerhold et al., 2008; Hilgen et al., 2015). Onshore sections also give different results, notably with the double isotopic excursion at ~59.3 and ~59 Ma in



the Tethys Himalaya (Li et al., 2024) and northwest Argentina (Hyland et al., 2015). Whereas all these studies agree on the short duration of the ELPE (< 1 million year), the difference between ages attributed to onshore and deep-sea sites highlight questions about the correlation between shallow and deep-sea carbonate sections.

3.3 Biogenic silica accumulation in the early late Palaeocene

In order to assess whether a signal corresponding to the ELPE is present in our records, we investigated the original drilling reports to find evidence of the various events indicative of this event. Six sites cover the presumed ELPE stratigraphic interval: 384, 700B, 752A, 1050A, 1051A and 1121B. In the North Atlantic, only Site 384 includes well-documented (Shipboard Scientific Party, 1979) record of a potential event occurring around the Selandian–Thanetian boundary. The report indicates that around this period, smear slide data reveal the presence of 1 to 2% of amorphous iron oxide and/or haematite in the nannofossil ooze, which enhances iron concentrations in the sediments. A severe foraminiferal dissolution event is also reported in Cores 384-8R and -9R, but this does not appear to affect nannofossils, hence the lack of prominent carbonate dissolution in the results (Fig. 2c). This event occurs before the peak in biosiliceous flux (Fig. 3a), in core section 384-7-6, which precedes a positive carbon excursion at ~57 Ma, accompanied by a drop in temperature (Boersma et al., 1979). This positive CIE could represent the onset of the PCIM, with the biosiliceous flux peak (Fig. 3a) occurring between the foraminiferal dissolution and the PCIM. In Hole 1051A, carbonate dissolution (Fig. 2c) also precedes the peak in biosiliceous content (Fig. 3a) and occurs at the same level as the peaks in magnetic susceptibility and iron, used by Westerhold et al. (2008) to determine the ELPE at this site. However, in the nearby Hole 1050A, bioSiO_2 flux (Fig. 3a) and magnetic susceptibility (Shipboard Scientific Party, 1998a) both increase with decreasing CaCO_3 percentage (Fig. 2c).

In the South Atlantic, the increase in $\delta^{13}\text{C}$ (Fig. 2b) at Hole 700B occurs after the peak of biosiliceous flux (Fig. 3b), as at Site 384. The resolution of the % CaCO_3 record in Fig. 2c is too coarse to define a proper dissolution interval, but (Shipboard Scientific Party, 1988) report that the carbonate dissolution event takes place in Core 700B-28R, as does the peak in biosiliceous content (Fig. 3b), and that benthic foraminiferal assemblages disappear from Cores 29R to 26R, while siliceous microfossils are abundant in Cores 32R to 26R. Furthermore, at the depth of the biosiliceous peak, the authors report the presence of anomalies in the gamma-ray record, with an increase in radioactivity derived mainly from uranium. Gamma-ray values are also high at Hole 752A (Indian Ocean), probably due to the presence of clay minerals derived from ash alteration (Shipboard Scientific Party, 1989), except in the core where the biosiliceous peak occurs (Fig. 3c). At this site, an abrupt shift in isotopic values (Figs 2a-b) occurs when biosiliceous flux values are the highest (Fig. 3c) and carbonate content is reduced (Fig. 2c).

For Hole 1121B, in the South Pacific, we compared our geochemical data with those of Hollis et al. (2014). A statistical comparison of the datasets (Pearson coefficient = 0.301) shows that despite a difference in resolution, the data are well aligned with each other (Fig. 2a–b), and it is therefore possible to use the higher resolution isotopic data from Hollis et al. (2014) in our study. At this site, each proxy record displays several peaks (Figs 2–3d) just after the Selandian–Thanetian boundary. Two carbonate dissolution events appear to have occurred (Fig. 2c), along with negative carbonate isotopic excursions (Fig. 2b) and peaks in bioSiO_2 content (Fig. 3d). (Shipboard Scientific Party, 2000) interpret the decrease in carbonate content as the result of CCD shoaling, possibly due to an inflow of cold-water masses, corrosive to carbonates.



Although some of the stages associated with the ELPE are present at the sites discussed in this study, the stratigraphy and/or identification of the event appear to be uncertain at our sites. This is highlighted by the results of the cross-correlations (see Supplementary Material Figs S2–22 and Table S1), showing that peaks between 57 and 60 Ma are correlated, but not precisely aligned with each other. Furthermore, the increase in biosiliceous flux does not always occur at the time of the carbonate dissolution, but sometimes precedes it, as indicated by the Pearson coefficient (Pearson coefficient between bioSiO_2 and $\%\text{CaCO}_3$: 0.462 at Site 384, -0.086 at Hole 700B, -0.646 at Hole 752A, -0.712 at Hole 1050A, 0.047 at Hole 1051A and -0.297 at Hole 1121B). The various results produced for this study are therefore not sufficiently significant to clearly link the increase in bioSiO_2 to the ELPE, but it seems that siliceous microfossils became abundant after the Selandian–Thanetian boundary, for a short period of time. The differences in timing of the ELPE between sites could potentially be related to an error in the calibration of the updated age-depth models, or reveal the occurrence of several short-lived ocean changes during this interval. However, such a calibration error is a less plausible explanation, as it would have to occur in each of the eight age-depth models to produce these delays, and the results are not delayed in this way for the LDE.

4 Conclusions

The two increases in biosiliceous fluxes during the Palaeocene appear to have occurred at similar times in the Atlantic, Pacific and Indian oceans. Although the correlation between the higher productivity of siliceous biota and the Latest Danian Event is strongly supported, the peaks in biosiliceous fluxes around the Selandian–Thanetian boundary should be interpreted with caution. The uncertain stratigraphy at the sites studied make it difficult to effectively link an increase in biosilica to the Early Late Palaeocene Event, in particular as the response of siliceous microfossils to the ELPE and LDE has not yet been investigated.

Data availability. The results of biogenic opal determination and isotopic measurements can be found in the Supplementary Material Table S4.

Author contributions. JW designed the study. CF and JW prepared the samples and carried out the biogenic opal determination. SB carried out the stable isotope analysis. JR processed the data. All co-authors participated in the interpretation of the data. CF prepared the paper, with contributions from all co-authors.

Competing interests. The authors declare that they have no conflict of interest.

Acknowledgements. We would like to thank Danuta Cembrowska-Lech for her advice on statistical treatment.



References

- Alegret, L., Ortiz, S., Arreguín-Rodríguez, G. J., Monechi, S., Millán, I., and Molina, E.: Microfossil turnover across the up-
 200 permost Danian at Caravaca, Spain: Paleoenvironmental inferences and identification of the latest Danian event, 463, 45–59,
<https://doi.org/10.1016/j.palaeo.2016.09.013>, 2016.
- Barnet, J. S. K., Littler, K., Westerhold, T., Kroon, D., Leng, M. J., Bailey, I., Röhl, U., and Zachos, J. C.: A High-Fidelity Benthic Stable Iso-
 tope Record of Late Cretaceous–Early Eocene Climate Change and Carbon-Cycling, 34, 672–691, <https://doi.org/10.1029/2019PA003556>,
 2019.
- 205 Bernaola, G., Baceta, J. I., Orue-Etxebarria, X., Alegret, L., Martin-Rubio, M., Arostegui, J., and Dinares-Turell, J.: Evidence of
 an abrupt environmental disruption during the mid-Paleocene biotic event (Zumaia section, western Pyrenees), 119, 785–795,
<https://doi.org/10.1130/B26132.1>, 2007.
- Berner, R. A., Lasaga, A. C., and Garrels, R. M.: The carbonate-silicate geochemical cycle and its effect on atmospheric carbon dioxide over
 the past 100 million years, 283, 641–683, <https://doi.org/10.2475/ajs.283.7.641>, 1983.
- 210 Boersma, A., Shackleton, N. J., Hall, M., and Given, Q.: Carbon and oxygen isotope records at DSDP site 384 (North Atlantic) and some
 Paleocene paleotemperatures and carbon isotope variations in the Atlantic ocean, in: Initial Reports of the Deep Sea Drilling Project, 43,
 edited by Tucholke, B., Vogt, P., and et al., vol. 43 of *Initial Reports of the Deep Sea Drilling Project*, U.S. Government Printing Office,
<https://doi.org/10.2973/dsdp.proc.43.1979>, 1979.
- Bornemann, A., Schulte, P., Sprong, J., Steurbaut, E., Youssef, M., and Speijer, R. P.: Latest Danian carbon isotope anomaly and associated
 215 environmental change in the southern Tethys (Nile Basin, Egypt), 166, 1135–1142, <https://doi.org/10.1144/0016-76492008-104>, 2009.
- Bowen, G. J., Beerling, D. J., Koch, P. L., Zachos, J. C., and Quattlebaum, T.: A humid climate state during the Palaeocene/Eocene thermal
 maximum, 432, 495–499, <https://doi.org/10.1038/nature03115>, 2004.
- Bralower, T. J., Premoli Silva, I., Malone, M. J., and Scientific Participants Of Leg 198: New evidence for abrupt climate change in the Cre-
 taceous and Paleogene: An Ocean Drilling Program expedition to Shatsky Rise, northwest Pacific, 12, 4–10, [https://doi.org/10.1130/1052-5173\(2002\)012<0004:NEFACC>2.0.CO;2](https://doi.org/10.1130/1052-5173(2002)012<0004:NEFACC>2.0.CO;2), 2002.
- 220 Coccioni, R., Frontalini, F., Catanzariti, R., Jovane, L., Rodelli, D., Rodrigues, I. M., Savian, J. F., Giorgioni, M., and Galbrun, B.: Paleoen-
 vironmental signature of the Selandian–Thanetian Transition Event (STTE) and Early Late Paleocene Event (ELPE) in the Contessa Road
 section (western Neo-Tethys), 523, 62–77, <https://doi.org/10.1016/j.palaeo.2019.03.023>, 2019.
- Dinarès-Turell, J., Pujalte, V., Stoykova, K., Baceta, J. I., and Ivanov, M.: The Palaeocene “top chron C27n” transient greenhouse episode:
 225 evidence from marine pelagic Atlantic and peri-Tethyan sections, 24, 477–486, <https://doi.org/10.1111/j.1365-3121.2012.01086.x>, 2012.
- Figus, C., Renaudie, J., Bialik, O. M., and Witkowski, J.: Controls on Palaeogene deep-sea diatom-bearing sediment deposition and compar-
 ison with shallow marine environments, <https://doi.org/10.5194/egusphere-2024-3768>.
- Figus, C., Bialik, O. M., Gladenkov, A. Y., Oreshkina, T. V., Renaudie, J., Smirnov, P., and Witkowski, J.: Climatic and tectonic controls on
 shallow-marine and freshwater diatomite deposition throughout the Palaeogene, 20, 2629–2644, <https://doi.org/10.5194/cp-20-2629-2024>,
 230 2024.
- Foster, G. L., Royer, D. L., and Lunt, D. J.: Future climate forcing potentially without precedent in the last 420 million years, 8, 14 845,
<https://doi.org/10.1038/ncomms14845>, 2017.
- Foster, G. L., Hull, P., Lunt, D. J., and Zachos, J. C.: Placing our current ‘hyperthermal’ in the context of rapid climate change in our
 geological past, 376, 20170 086, <https://doi.org/10.1098/rsta.2017.0086>, 2018.



- 235 Froelich, F. and Misra, S.: Was the Late Paleocene-Early Eocene Hot Because Earth Was Flat? An Ocean Lithium Isotope View of Mountain Building, Continental Weathering, Carbon Dioxide, and Earth's Cenozoic Climate, 27, 36–49, <https://doi.org/10.5670/oceanog.2014.06>, 2014.
- Gradstein, F. M., Ogg, J. G., Schmitz, M., and Ogg, G.: The Geologic Time Scale 2012 2-Volume Set, Elsevier Science, ISBN 978-0-444-59448-8, OCLC: 956664433, 2012.
- 240 Green, P. J. and Silverman, B. W.: Nonparametric regression and generalized linear models: a roughness penalty approach, no. 58 in *Mono-graphs on statistics and applied probability*, Chapman & Hall, ISBN 978-0-412-30040-0, 1994.
- Haq, B. U., Hisatake, O., and Lohmann, G. P.: Paleobiogeography of the Paleocene/Eocene calcareous nannoplankton from the North Atlantic Ocean, in: *Initial Reports of the Deep Sea Drilling Project*, 43, edited by Tucholke, B., Vogt, P., and et al., vol. 43 of *Initial Reports of the Deep Sea Drilling Project*, U.S. Government Printing Office, <https://doi.org/10.2973/dsdp.proc.43.1979>, 1979.
- 245 Hilgen, F. J., Abels, H. A., Kuiper, K. F., Lourens, L. J., and Wolthers, M.: Towards a stable astronomical time scale for the Paleocene: Aligning Shatsky Rise with the Zumaia – Walvis Ridge ODP Site 1262 composite, 48, 91–110, <https://doi.org/10.1127/nos/2014/0054>, 2015.
- Hollis, C. J., Tayler, M. J., Andrew, B., Taylor, K. W., Lurcock, P., Bijl, P. K., Kulhanek, D. K., Crouch, E. M., Nelson, C. S., Pancost, R. D., Huber, M., Wilson, G. S., Ventura, G. T., Crampton, J. S., Schiøler, P., and Phillips, A.: Organic-rich sedimentation in the South Pacific Ocean associated with Late Paleocene climatic cooling, 134, 81–97, <https://doi.org/10.1016/j.earscirev.2014.03.006>, 2014.
- 250 Hollis, C. J., Naeher, S., Clowes, C. D., Naafs, B. D. A., Pancost, R. D., Taylor, K. W. R., Dahl, J., Li, X., Ventura, G. T., and Sykes, R.: Late Paleocene CO₂ drawdown, climatic cooling and terrestrial denudation in the southwest Pacific, 18, 1295–1320, <https://doi.org/10.5194/cp-18-1295-2022>, 2022.
- Hyland, E. G., Sheldon, N. D., and Cotton, J. M.: Terrestrial evidence for a two-stage mid-Paleocene biotic event, 417, 371–378, <https://doi.org/10.1016/j.palaeo.2014.09.031>, 2015.
- 255 Jehle, S., Bornemann, A., Deprez, A., and Speijer, R. P.: The Impact of the Latest Danian Event on Planktic Foraminiferal Faunas at ODP Site 1210 (Shatsky Rise, Pacific Ocean), 10, e0141644, <https://doi.org/10.1371/journal.pone.0141644>, 2015.
- Jehle, S., Bornemann, A., Lägler, A. F., Deprez, A., and Speijer, R. P.: Paleooceanographic changes across the Latest Danian Event in the South Atlantic Ocean and planktic foraminiferal response, 525, 1–13, <https://doi.org/10.1016/j.palaeo.2019.03.024>, 2019.
- 260 Kennett, J. P. and Stott, L. D.: Abrupt deep-sea warming, palaeoceanographic changes and benthic extinctions at the end of the Palaeocene, 353, 225–229, <https://doi.org/10.1038/353225a0>, 1991.
- Kiessling, W., Reddin, C. J., Dowding, E. M., Dimitrijević, D., Raja, N. B., and Kocsis, A. T.: Marine biological responses to abrupt climate change in deep time, pp. 1–15, <https://doi.org/10.1017/pab.2024.20>, 2024.
- Li, J., Hu, X., Garzanti, E., Boudagher-Fadel, M., Jiang, J., and Xu, Y.: The record of the Early Late Paleocene Event (ELPE, 59.5 Ma) in shallow-water Tethys Himalayan carbonates (Zongpu Formation, South Tibet), 94, 937–952, <https://doi.org/10.2110/jsr.2023.022>, 2024.
- 265 Littler, K., Röhl, U., Westerhold, T., and Zachos, J. C.: A high-resolution benthic stable-isotope record for the South Atlantic: Implications for orbital-scale changes in Late Paleocene–Early Eocene climate and carbon cycling, 401, 18–30, <https://doi.org/10.1016/j.epsl.2014.05.054>, 2014.
- McInerney, F. A. and Wing, S. L.: The Paleocene-Eocene Thermal Maximum: A Perturbation of Carbon Cycle, Climate, and Biosphere with Implications for the Future, 39, 489–516, <https://doi.org/10.1146/annurev-earth-040610-133431>, 2011.
- 270



- Olivarez Lyle, A. and Lyle, M.: Determination of biogenic opal in pelagic marine sediments: a simple method revisited, in: Proceedings of the Ocean Drilling Program, 199 Initial Reports, edited by Lyle, M., Wilson, P., Janecek, T., and et al., vol. 199 of *Proceedings of the Ocean Drilling Program*, Ocean Drilling Program, <https://doi.org/10.2973/odp.proc.ir.199.2002>, 2002.
- Penman, D. E.: Silicate weathering and North Atlantic silica burial during the Paleocene-Eocene Thermal Maximum, 44, 731–734, <https://doi.org/10.1130/G37704.1>, 2016.
- Penman, D. E., Hönisch, B., Zeebe, R. E., Thomas, E., and Zachos, J. C.: Rapid and sustained surface ocean acidification during the Paleocene-Eocene Thermal Maximum, 29, 357–369, <https://doi.org/10.1002/2014PA002621>, 2014.
- Penman, D. E., Keller, A., D’haenens, S., Kirtland Turner, S., and Hull, P. M.: Atlantic Deep-Sea Cherts Associated With Eocene Hyperthermal Events, 34, 287–299, <https://doi.org/10.1029/2018PA003503>, 2019.
- 280 Petrizzo, M. R.: An Early Late Paleocene Event on Shatsky Rise, northwest Pacific ocean (ODP Leg 198): evidence from planktonic foraminiferal assemblages, in: Proceedings of the Ocean Drilling Program, 198 Scientific Results, edited by Bralower, T., Premoli Silva, I., and Malone, M., vol. 198 of *Proceedings of the Ocean Drilling Program*, Ocean Drilling Program, <https://doi.org/10.2973/odp.proc.sr.198.2006>, 2006.
- R Core Team: R: A Language and Environment for Statistical Computing, R Foundation for Statistical Computing, Vienna, Austria, <https://www.R-project.org/>, 2024.
- 285 Renaudie, J., Drews, E.-L., and Böhne, S.: The Paleocene record of marine diatoms in deep-sea sediments, 21, 183–205, <https://doi.org/10.5194/fr-21-183-2018>, 2018.
- Rice, S., Freund, H., Huang, W., Clouse, J., and Isaacs, C.: Application of Fourier Transform Infrared Spectroscopy to Silica Diagenesis: The Opal-A to Opal-Ct Transformation, Vol. 65A, 639–647, <https://doi.org/10.1306/D4268185-2B26-11D7-8648000102C1865D>, 1995.
- 290 Sarkar, S., Cotton, L. J., Valdes, P. J., and Schmidt, D. N.: Shallow Water Records of the PETM: Novel Insights From NE India (Eastern Tethys), 37, e2021PA004 257, <https://doi.org/10.1029/2021PA004257>, 2022.
- Shipboard Scientific Party: Site 208, in: Initial Reports of the Deep Sea Drilling Project, 21, edited by Burns, J., Andrews, J., and et al., vol. 21 of *Initial Reports of the Deep Sea Drilling Project*, U.S. Government Printing Office, <https://doi.org/10.2973/dsdp.proc.21.1973>, 1973.
- 295 Shipboard Scientific Party: Site 384: the Cretaceous/Tertiary boundary, Aptian reefs, and the J-Anomaly Ridge, in: Initial Reports of the Deep Sea Drilling Project, 43, edited by Tucholke, B., Vogt, P., and et al., vol. 43 of *Initial Reports of the Deep Sea Drilling Project*, U.S. Government Printing Office, <https://doi.org/10.2973/dsdp.proc.43.1979>, 1979.
- Shipboard Scientific Party: Site 700, in: Proceedings of the Ocean Drilling Program, 114 Initial Reports, edited by Ciesielski, P., Kristoffersen, Y., and et al., vol. 114 of *Proceedings of the Ocean Drilling Program*, Ocean Drilling Program, <https://doi.org/10.2973/odp.proc.ir.114.1988>, 1988.
- 300 Shipboard Scientific Party: Site 752, in: Proceedings of the Ocean Drilling Program, 121 Initial Reports, edited by Peirce, J., Weissel, J., and et al., vol. 121 of *Proceedings of the Ocean Drilling Program*, Ocean Drilling Program, <https://doi.org/10.2973/odp.proc.ir.121.1989>, 1989.
- Shipboard Scientific Party: Site 1050, in: Proceedings of the Ocean Drilling Program 171B Initial Reports, edited by Norris, R., Kroon, D., Klaus, A., and et al., vol. 171B of *Proceedings of the Ocean Drilling Program*, Ocean Drilling Program, <https://doi.org/10.2973/odp.proc.ir.171B.1998>, 1998a.
- 305



- Shipboard Scientific Party: Site 1051, in: Proceedings of the Ocean Drilling Program 171B Initial Reports, edited by Norris, R., Kroon, D., Klaus, A., and et al., vol. 171B of *Proceedings of the Ocean Drilling Program*, Ocean Drilling Program, <https://doi.org/10.2973/odp.proc.ir.171B.1998, 1998b>.
- 310 Shipboard Scientific Party: Site 1121: the Campbell "Drift", in: Proceedings of the Ocean Drilling Program, 181 Initial Reports, edited by Carter, R., McCave, I., Richter, C., Carter, L., and et al., vol. 181 of *Proceedings of the Ocean Drilling Program*, Ocean Drilling Program, <https://doi.org/10.2973/odp.proc.ir.181.2000, 2000>.
- Sprong, J., Kouwenhoven, T. J., Bornemann, A., Schulte, P., Stassen, P., Steurbaut, E., Youssef, M., and Speijer, R. P.: Characterization of the Latest Danian Event by means of benthic foraminiferal assemblages along a depth transect at the southern Tethyan margin (Nile Basin, Egypt), 86–87, 15–31, <https://doi.org/10.1016/j.marmicro.2012.01.001, 2012>.
- 315 Westerhold, T., Röhl, U., Raffi, I., Fornaciari, E., Monechi, S., Reale, V., Bowles, J., and Evans, H. F.: Astronomical calibration of the Paleocene time, 257, 377–403, <https://doi.org/10.1016/j.palaeo.2007.09.016, 2008>.
- Westerhold, T., Röhl, U., Donner, B., and Zachos, J. C.: Global Extent of Early Eocene Hyperthermal Events: A New Pacific Benthic Foraminiferal Isotope Record From Shatsky Rise (ODP Site 1209), 33, 626–642, <https://doi.org/10.1029/2017PA003306, 2018>.
- 320 Westerhold, T., Marwan, N., Drury, A. J., Liebrand, D., Agnini, C., Anagnostou, E., Barnet, J. S. K., Bohaty, S. M., De Vleeschouwer, D., Florindo, F., Frederichs, T., Hodell, D. A., Holbourn, A. E., Kroon, D., Lauretano, V., Littler, K., Lourens, L. J., Lyle, M., Pälike, H., Röhl, U., Tian, J., Wilkens, R. H., Wilson, P. A., and Zachos, J. C.: An astronomically dated record of Earth's climate and its predictability over the last 66 million years, 369, 1383–1387, <https://doi.org/10.1126/science.aba6853, 2020>.
- Witkowski, J., Penman, D. E., Brylka, K., Wade, B. S., Matting, S., Harwood, D. M., and Bohaty, S. M.: Early Paleogene biosiliceous sedimentation in the Atlantic Ocean: Testing the inorganic origin hypothesis for Paleocene and Eocene chert and porcellanite, 556, 109 896, <https://doi.org/10.1016/j.palaeo.2020.109896, 2020>.
- 325 Witkowski, J., Brylka, K., Bohaty, S. M., Mydlowska, E., Penman, D. E., and Wade, B. S.: North Atlantic marine biogenic silica accumulation through the early to middle Paleogene: implications for ocean circulation and silicate weathering feedback, 17, 1937–1954, <https://doi.org/10.5194/cp-17-1937-2021, 2021>.
- 330 Yanchilina, A., Yam, R., Kolodny, Y., and Shemesh, A.: From diatom opal-A $\delta^{18}\text{O}$ to chert $\delta^{18}\text{O}$ in deep sea sediments, 268, 368–382, <https://doi.org/10.1016/j.gca.2019.10.018, 2020>.
- Zachos, J. C., Dickens, G. R., and Zeebe, R. E.: An early Cenozoic perspective on greenhouse warming and carbon-cycle dynamics, 451, 279–283, <https://doi.org/10.1038/nature06588, 2008>.

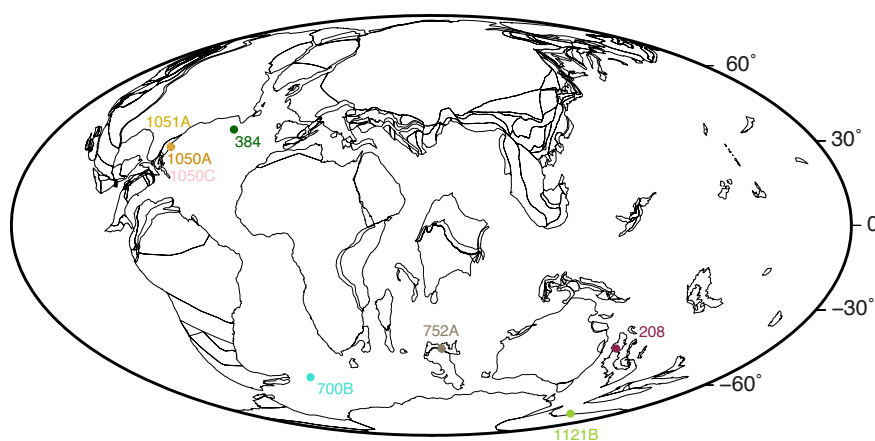


Figure 1. Palaeogeographic map of the site locations at ~60 Ma. Map generated on the Ocean Drilling Stratigraphic Network Advanced Plate Tectonic Reconstruction service (www.odsn.de).

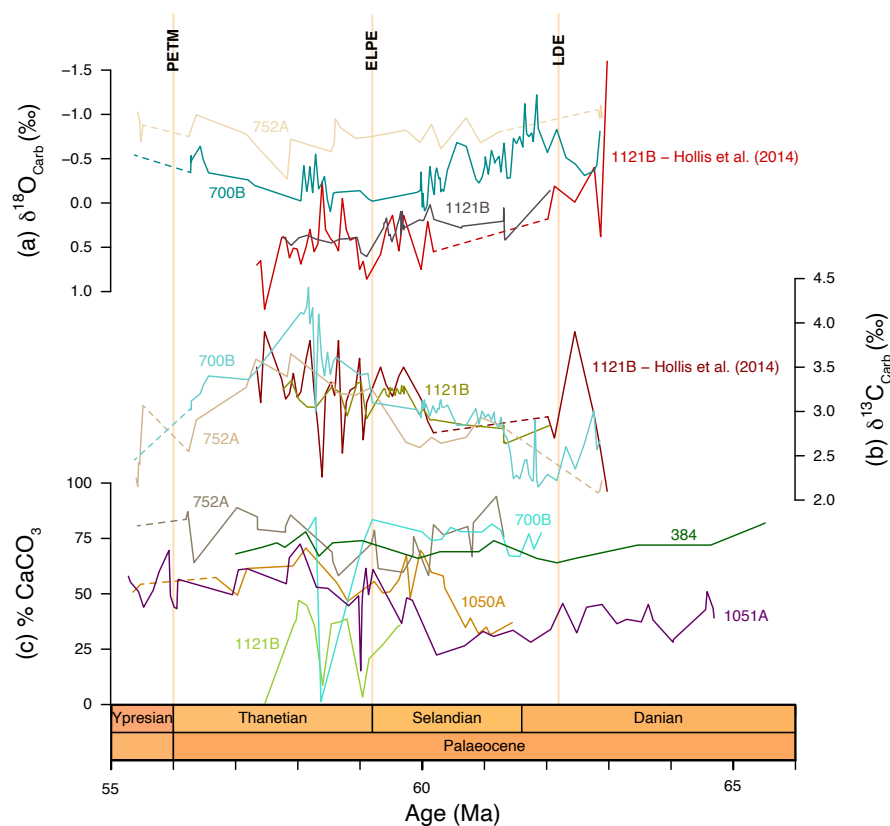


Figure 2. Comparison of measured (a) $\delta^{18}\text{O}$ and (b) $\delta^{13}\text{C}$ in ‰ at sites 700B, 752A and 1121B with results from Hollis et al. (2014). (c) Percent CaCO_3 values at the study sites from the International Ocean Discovery Program Janus database (web.iodp.tamu.edu). PETM: Palaeocene Eocene Thermal Maximum (~56 Ma), ELPE: Early Late Palaeocene Event (~59.2 Ma), LDE: Latest Danian Event (~62.2 Ma).

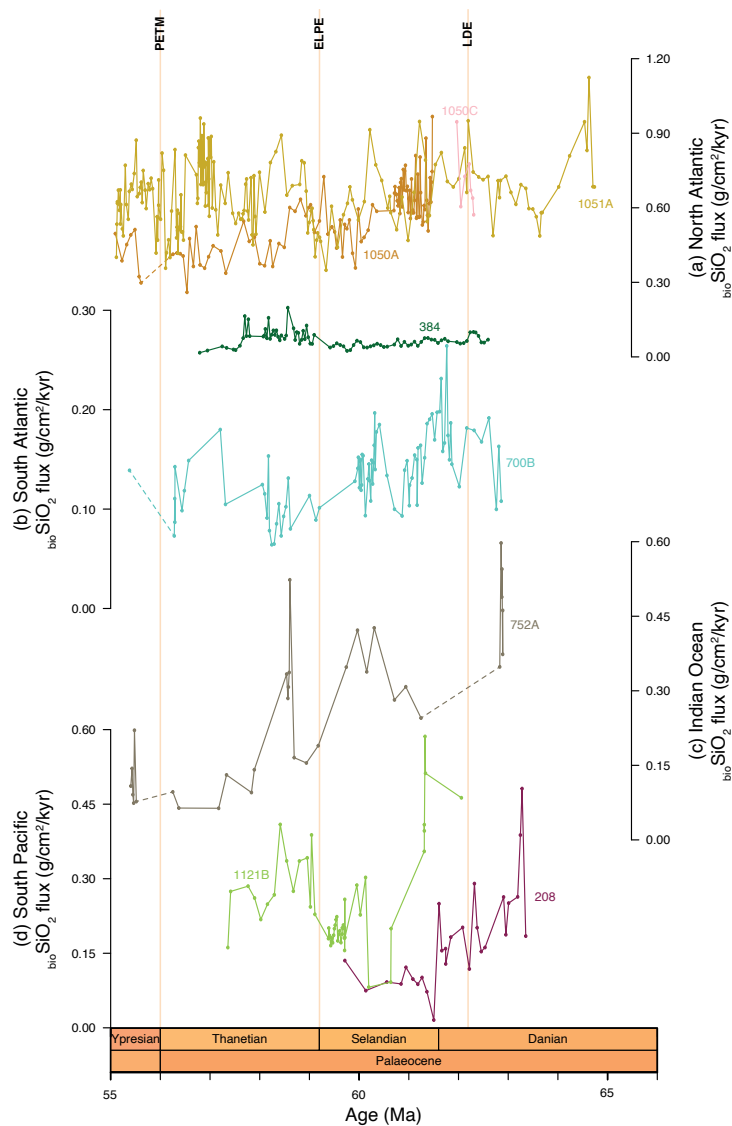


Figure 3. bioSiO_2 fluxes measured in $\text{g/cm}^2/\text{kyr}$ at study sites in the (a) North Atlantic, (b) South Atlantic, (c) Indian Ocean and (d) South Pacific. Results for sites 1050A, 1050C and 1051A are from Witkowski et al. (2021).